Formation of chiral fields in a symmetric environment

Martin Schäferling,* Xinghui Yin, and Harald Giessen

4th Physics Institute, Research Center SCoPE, and Research Center SimTech, University of Stuttgart, Pfaffenwaldring 57, 70569 Stuttgart, Germany

**m.schaeferling@pi4.uni-stuttgart.de*

Abstract: Chiral fields, i. e., electromagnetic fields with nonvanishing optical chirality, can occur next to symmetric nanostructures without geometrical chirality illuminated with linearly polarized light at normal incidence. A simple dipole model is utilized to explain this behavior theoretically. Illuminated with circularly polarized light, the chiral near-fields are still dominated by the distributions found for the linear polarization but show additional features due to the optical chirality of the incident light. Rotating the angle of linear polarization introduces more subtle changes to the distribution of optical chirality. Using our findings, we propose a novel scheme to obtain chiroptical far-field response using linearly polarized light, which could be utilized for applications such as optical enantiomer sensing.

OCIS codes: (250.5403) Plasmonics; (310.5448) Polarization, other optical properties; (350.4238) Nanophotonics and photonic crystals.

References and links

1. L. D. Barron, *Molecular Light Scattering and Optical Activity* (Cambridge University Press, 2004), 2nd ed.
2. B. K. Canfield, S. Kujala, K. Laiho, K. Jefimovs, J. Turunen, and M. Kauranen, "Chirality arising from small defects in gold nanoparticle arrays," Opt. Express **14**, 950–955 (2006).
3. S. Zhang, H. Wei, K. Bao, U. Håkanson, N. Halas, P. Nordlander, and H. Xu, "Chiral surface plasmon polaritons on metallic nanowires," Phys. Rev. Lett. **107**, 096801 (2011).
4. A. Guerrero-Martínez, J. L. Alonso-Gómez, B. Auguié, M. M. Cid, and L. M. Liz-Marzán, "From individual to collective chirality in metal nanoparticles," Nano Today **6**, 381–400 (2011).
5. Z. Fan and A. O. Govorov, "Chiral nanocrystals: plasmonic spectra and circular dichroism." Nano Lett. **12**, 3283–3289 (2012).
6. F. Eftekhari and T. J. Davis, "Strong chiral optical response from planar arrays of subwavelength metallic structures supporting surface plasmon resonances," Phys. Rev. B **86**, 075428 (2012).
7. A. Christofi, N. Stefanou, G. Gantzounis, and N. Papanikolaou, "Giant optical activity of helical architectures of plasmonic nanorods," J. Phys. Chem. C **116**, 16674–16679 (2012).
8. A. Papakostas, A. Potts, D. Bagnall, S. Prosvirnin, H. Coles, and N. Zheludev, "Optical manifestations of planar chirality," Phys. Rev. Lett. **90**, 107404 (2003).
9. M. Kuwata-Gonokami, N. Saito, Y. Ino, M. Kauranen, K. Jefimovs, T. Vallius, J. Turunen, and Y. Svirko, "Giant optical activity in quasi-two-dimensional planar nanostructures," Phys. Rev. Lett. **95**, 227401 (2005).
10. E. Plum, X.-X. Liu, V. Fedotov, Y. Chen, D. Tsai, and N. Zheludev, "Metamaterials: optical activity without chirality," Phys. Rev. Lett. **102**, 113902 (2009).
11. V. K. Valev, N. Smisdom, A. V. Silhanek, B. De Clercq, W. Gillijns, M. Ameloot, V. V. Moshchalkov, and T. Verbiest, "Plasmonic ratchet wheels: switching circular dichroism by arranging chiral nanostructures." Nano Lett. **9**, 3945–3948 (2009).
12. A. V. Rogacheva, V. A. Fedotov, A. S. Schwanecke, and N. I. Zheludev, "Giant gyrotropy due to electromagnetic-field coupling in a bilayered chiral structure," Phys. Rev. Lett. **97**, 177401 (2006).
13. M. Decker, M. W. Klein, M. Wegener, and S. Linden, "Circular dichroism of planar chiral magnetic metamaterials," Opt. Lett. **32**, 856–858 (2007).

#176581 - $15.00 USD Received 20 Sep 2012; revised 31 Oct 2012; accepted 1 Nov 2012; published 7 Nov 2012

14. M. Decker, M. Ruther, C. E. Kriegler, J. Zhou, C. M. Soukoulis, S. Linden, and M. Wegener, "Strong optical activity from twisted-cross photonic metamaterials," Opt. Lett. **34**, 2501–2503 (2009).
15. N. Liu, H. Liu, S. Zhu, and H. Giessen, "Stereometamaterials," Nat. Photon. **3**, 157–162 (2009).
16. C. Menzel, C. Helgert, C. Rockstuhl, E.-B. Kley, A. Tünnermann, T. Pertsch, and F. Lederer, "Asymmetric transmission of linearly polarized light at optical metamaterials," Phys. Rev. Lett. **104**, 253902 (2010).
17. M. Decker, R. Zhao, C. M. Soukoulis, S. Linden, and M. Wegener, "Twisted split-ring-resonator photonic metamaterial with huge optical activity," Opt. Lett. **35**, 1593–1596 (2010).
18. R. Zhao, L. Zhang, J. Zhou, T. Koschny, and C. Soukoulis, "Conjugated gammadion chiral metamaterial with uniaxial optical activity and negative refractive index," Phys. Rev. B **83**, 035105 (2011).
19. C. Helgert, E. Pshenay-Severin, M. Falkner, C. Menzel, C. Rockstuhl, E. B. Kley, A. Tuennermann, F. Lederer, and T. Pertsch, "Chiral metamaterial composed of three-dimensional plasmonic nanostructures." Nano Lett. **11**, 4400–4404 (2011).
20. M. Hentschel, M. Schäferling, T. Weiss, N. Liu, and H. Giessen, "Three-dimensional chiral plasmonic oligomers." Nano Lett. **12**, 2542–2547 (2012).
21. Y. Zhao, M. A. Belkin, and A. Alù, "Twisted optical metamaterials for planarized ultrathin broadband circular polarizers." Nat. Commun. **3**, 870 (2012).
22. J. K. Gansel, M. Thiel, M. S. Rill, M. Decker, K. Bade, V. Saile, G. von Freymann, S. Linden, and M. Wegener, "Gold helix photonic metamaterial as broadband circular polarizer." Science **325**, 1513–1515 (2009).
23. A. Radke, T. Gissibl, T. Klotzbücher, P. V. Braun, and H. Giessen, "3D Bichiral Plasmonic Crystals: Three-Dimensional bichiral plasmonic crystals fabricated by direct laser writing and electroless silver plating (Adv. Mater. 27/2011)." Adv. Mater. **23**, 2995–3021 (2011).
24. A. Guerrero-Martínez, B. Auguié, J. L. Alonso-Gómez, Z. Džolić, S. Gómez-Graña, M. Žinić, M. M. Cid, and L. M. Liz-Marzán, "Intense optical activity from three-dimensional chiral ordering of plasmonic nanoantennas," Angew. Chemie Int. Ed. **123**, 5613–5617 (2011).
25. A. Kuzyk, R. Schreiber, Z. Fan, G. Pardatscher, E.-M. Roller, A. Högele, F. C. Simmel, A. O. Govorov, and T. Liedl, "DNA-based self-assembly of chiral plasmonic nanostructures with tailored optical response." Nature **483**, 311–314 (2012).
26. J. K. Gansel, M. Latzel, A. Frölich, J. Kaschke, M. Thiel, and M. Wegener, "Tapered gold-helix metamaterials as improved circular polarizers," Appl. Phys. Lett. **100**, 101109 (2012).
27. X. Shen, C. Song, J. Wang, D. Shi, Z. Wang, N. Liu, and B. Ding, "Rolling up gold nanoparticle-dressed DNA origami into three-dimensional plasmonic chiral nanostructures." J. Am. Chem. Soc. **134**, 146–149 (2012).
28. E. Hendry, T. Carpy, J. Johnston, M. Popland, R. V. Mikhaylovskiy, A. J. Lapthorn, S. M. Kelly, L. D. Barron, N. Gadegaard, and M. Kadodwala, "Ultrasensitive detection and characterization of biomolecules using superchiral fields." Nat. Nanotechnol. **5**, 783–787 (2010).
29. A. O. Govorov, Z. Fan, P. Hernandez, J. M. Slocik, and R. R. Naik, "Theory of circular dichroism of nanomaterials comprising chiral molecules and nanocrystals: plasmon enhancement, dipole interactions, and dielectric effects." Nano Lett. **10**, 1374–1382 (2010).
30. J. M. Slocik, A. O. Govorov, and R. R. Naik, "Plasmonic circular dichroism of peptide-functionalized gold nanoparticles," Nano Lett. **11**, 701–705 (2011).
31. A. O. Govorov, "Plasmon-induced circular dichroism of a chiral molecule in the vicinity of metal nanocrystals. Application to various geometries," J. Phys. Chem. C **115**, 7914–7923 (2011).
32. V. A. Gérard, Y. K. Gun'ko, E. Defrancq, and A. O. Govorov, "Plasmon-induced CD response of oligonucleotide-conjugated metal nanoparticles." Chem. Comm. **47**, 7383–7385 (2011).
33. N. Abdulrahman, Z. Fan, T. Tonooka, S. Kelly, N. Gadegaard, E. Hendry, A. O. Govorov, and M. Kadodwala, "Induced chirality through electromagnetic coupling between chiral molecular layers and plasmonic nanostructures." Nano Lett. **12**, 977–983 (2012).
34. A. O. Govorov and Z. Fan, "Theory of chiral plasmonic nanostructures comprising metal nanocrystals and chiral molecular media." Chem. Phys. Chem. **13**, 2551–2560 (2012).
35. D. M. Lipkin, "Existence of a new conservation law in electromagnetic theory," J. Math. Phys. **5**, 696–674 (1964).
36. Y. Tang and A. E. Cohen, "Optical chirality and its interaction with matter," Phys. Rev. Lett. **104**, 163901 (2010).
37. Y. Tang and A. E. Cohen, "Enhanced enantioselectivity in excitation of chiral molecules by superchiral light." Science **332**, 333–336 (2011).
38. K. Bliokh and F. Nori, "Characterizing optical chirality," Phys. Rev. A **83**, 021803 (2011).
39. S. A. Maier and H. A. Atwater, "Plasmonics: localization and guiding of electromagnetic energy in metal/dielectric structures," J. Appl. Phys **98**, 011101 (2005).
40. S. Lal, S. Link, and N. J. Halas, "Nano-optics from sensing to waveguiding," Nat. Photon. **1**, 641–648 (2007).
41. J. A. Schuller, E. S. Barnard, W. Cai, Y. C. Jun, J. S. White, and M. L. Brongersma, "Plasmonics for extreme light concentration and manipulation." Nat. Mater. **9**, 193–204 (2010).
42. N. J. Halas, S. Lal, W.-S. Chang, S. Link, and P. Nordlander, "Plasmons in strongly coupled metallic nanostructures." Chem. Rev. **111**, 3913–3961 (2011).
43. M. Schäferling, D. Dregely, M. Hentschel, and H. Giessen, "Tailoring enhanced optical chirality: design principles for chiral plasmonic nanostructures," Phys. Rev. X **2**, 031010 (2012).

#176581 - $15.00 USD Received 20 Sep 2012; revised 31 Oct 2012; accepted 1 Nov 2012; published 7 Nov 2012

44. S. V. Zhukovsky, C. Kremers, and D. N. Chigrin, "Plasmonic rod dimers as elementary planar chiral meta-atoms," Opt. Lett. **36**, 2278–2280 (2011).
45. D. N. Chigrin, C. Kremers, and S. V. Zhukovsky, "Plasmonic nanoparticle monomers and dimers: from nanoantennas to chiral metamaterials," Appl. Phys. B **105**, 81–97 (2011).
46. E. Hendry, R. V. Mikhaylovskiy, L. D. Barron, M. Kadodwala, and T. J. Davis, "Chiral electromagnetic fields generated by arrays of nanoslits." Nano Lett. **12**, 3640–3644 (2012).
47. S. Takahashia, A. Potts, D. Bagnall, N. I. Zheludev, and A. V. Zayats, "Near-field polarization conversion in planar chiral nanostructures," Opt. Commun. **255**, 91 (2005).
48. K. Konishi, M. Nomura, N. Kumagai, S. Iwamoto, Y. Arakawa, and M Kuwata-Gonokami, "Circularly polarized light emission from semiconductor planar chiral nanostructures," Phys. Rev. Lett. **106**, 057402 (2011).
49. P. Biagioni, M. Savoini, J.-S. Huang, L. Duò, M. Finazzi, and B. Hecht, "Near-field polarization shaping by a near-resonant plasmonic cross antenna," Phys. Rev. B. **80**, 153409 (2009).
50. T. Weiss, G. Granet, N. A. Gippius, S. G. Tikhodeev, and H. Giessen, "Matched coordinates and adaptive spatial resolution in the Fourier modal method," Opt. Expr. **17**, 8051–8061 (2009).
51. B. Gompf, J. Braun, T. Weiss, H. Giessen, M. Dressel, and U. Hübner, "Periodic nanostructures: spatial dispersion mimics chirality," Phys. Rev. Lett. **106**, 185501 (2011).
52. T. Weiss, N. A. Gippius, S. G. Tikhodeev, G. Granet, and H. Giessen, "Derivation of plasmonic resonances in the Fourier modal method with adaptive spatial resolution and matched coordinates," J. Opt. Soc. Am. A **28**, 238–244 (2011).
53. J. D. Jackson, *Classical Electrodynamics* (Wiley-VCH, 1998), 3rd ed.
54. L. Novotny, "Effective wavelength scaling for optical antennas," Phys. Rev. Lett. **98**, 266802 (2007).
55. J. Dorfmüller, R. Vogelgesang, W. Khunsin, C. Rockstuhl, C. Etrich, and K. Kern, "Plasmonic nanowire antennas: experiment, simulation, and theory." Nano Lett. **10**, 3596–3603 (2010).
56. N. Berova, K. Nakanishi, and R. W. Woody, eds., *Circular Dichroism: Principles and Applications* (Wiley-VCH, 2000), 2nd ed.

1. Introduction

Geometrical chirality – the absence of mirror symmetry – is an integral component of our world. For example, most biomolecules such as essential amino acids are chiral in that sense. The two mirror-symmetric enantiomers of a geometrically chiral object differ only in their handedness. Interaction with circularly polarized light, which is also chiral, causes effects such as circular dichroism and optical rotatory dispersion [1]. This chiroptical far-field response is a consequence of geometrical chirality.

In recent years, the concept of chirality has gathered substantial attention in the field of plasmonics [2–7]. Artificial geometrically chiral nanostructures with huge chiroptical far-field responses were reported in planar [8–11], bi- and multilayered [12–21], and even three-dimensional geometries [22–27]. First results also indicate that plasmonic nanostructures can enhance the interaction of chiral molecules placed in the vicinity of the structure with circularly polarized light, which is a route to highly sensitive enantiomer sensing [28–34].

For such applications, not only the chiroptical far-field response but the chiroptical near-field response of plasmonic nanostructures is of major importance. It can be quantified using the so-called optical chirality [35–38]

$$C = -\frac{\varepsilon_0 \omega}{2} \mathrm{Im}(\mathbf{E}^* \cdot \mathbf{B}), \tag{1}$$

which can be calculated for any monochromatic electromagnetic field. However, optical chirality should not be confused with the general geometrical concept of chirality. While the latter describes the mathematical concept of the absence of mirror symmetry within the structure, optical chirality is a physical property of an electromagnetic field. The link to the geometrical concept of chirality is established because the definition given in Eq.(1) fulfills the same symmetry constraints as geometrical chirality: optical chirality is a scalar value that is even in time and odd in parity. In the following, the term "chiral field" refers to electromagnetic fields with nonzero optical chirality, while the geometrical concept of chirality is addressed by "geometrical chirality".

#176581 - $15.00 USD Received 20 Sep 2012; revised 31 Oct 2012; accepted 1 Nov 2012; published 7 Nov 2012

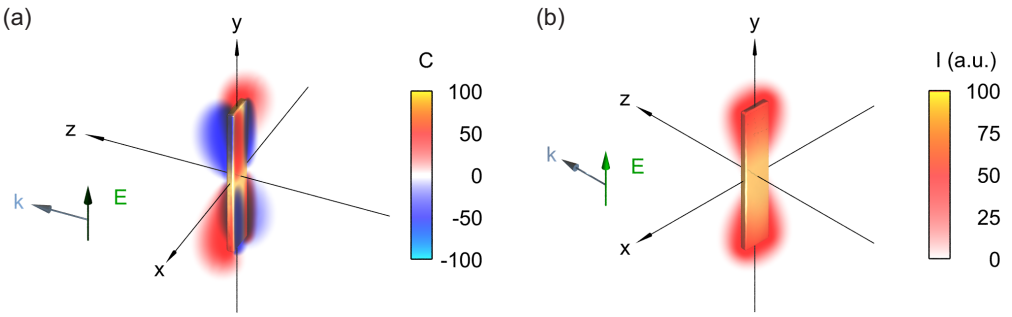

Fig. 1. (a) Optical chirality induced by a linear plasmonic nanoantenna illuminated with light polarized parallel to the antenna axis under normal incidence at resonance (217 THz). The values have been normalized by the optical chirality of circularly polarized light. (b) The fundamental antenna mode exhibits strongest intensity of the electric field at the ends of the rod. The distribution differs significantly from the regions with strongest optical chirality.

The optical chirality of plane waves depends on their polarization state. Maximum optical chirality is reached for circularly polarized light, which is also geometrically chiral as the field vectors are arranged helically in space:

$$C^{\mathrm{CPL}} = \pm \frac{\varepsilon_0 \omega}{2c} |\mathbf{E}|^2 \,. \tag{2}$$

Positive optical chirality corresponds to left-handed, negative one to right-handed circularly polarized light, respectively. It depends on both the intensity as well as the frequency of the wave. Similar to the electric field enhancement in plasmonic nanostructures [39–42], the optical chirality can be enhanced in the near-field of such structures. It has been found that structures with strong planar or three-dimensional geometrical chirality show the highest enhancement of optical chirality [43]. These structures would also lead to some chiroptical far-field response, namely either circular dichroism for three-dimensional geometrically chiral structures, or circular conversion dichroism for structures featuring planar geometrical chirality [44, 45].

Equation (1) indicates that one needs two prerequisites to obtain chiral near-fields: First, some component of the electric field vector must be parallel to the magnetic field vector. Second, these components must not be in phase. Recently, Hendry et al. demonstrated a very simple design where a lateral shift between two slits in a metallic film ensures the required relations between the electric and magnetic near-fields of the single slits [46]. This arrangement leads to planar geometrical chirality, and its handedness determines the handedness of the chiral fields. Earlier work also indicates that planar geometrically chiral structures can lead to local chiral fields [47, 48].

By now, to the best of our knowledge, no chiroptical far-field response has been reported for structures without geometrical chirality. Chiral near-fields, on the other hand, have been found in the vicinity of geometrically achiral structures [49]. However, a three-dimensional geometrically chiral situation was formed in combination with the incident polarization. We show in this paper that chiral near-fields can be even formed under conditions without any geometrical chirality at all.

2. Optical chirality of a plasmonic rod antenna

We consider a linear plasmonic gold nanoantenna that exhibits neither three-dimensional nor planar geometrical chirality. Therefore, no chiroptical far-field response can be obtained. The

#176581 - $15.00 USD Received 20 Sep 2012; revised 31 Oct 2012; accepted 1 Nov 2012; published 7 Nov 2012

structure is illuminated with linearly polarized light where the electric field vector is parallel to the antenna axis. The combination of structure and incident polarization exhibits no geometrical chirality. The results for this configuration can be seen in Fig. 1(a), which depicts the optical chirality near the nanoantenna. Local chiral fields that arise from this geometrically achiral system are clearly visible.

The dimensions of the antenna are 200 nm in length and 80 nm in width with a thickness of 20 nm which leads to a resonance at 217 THz. The fields were calculated using a FMM-based Maxwell solver with a Drude model for gold [50]. The resulting optical chirality was normalized by the absolute values obtained for circularly polarized incident light (cf. Eq. (2)) at the same frequency without the nanostructure. Thus, the calculated values are independent of frequency as well as intensity of the incident light. Both the structure as well as the incident light are achiral in both two and three dimensions. Also, influences from spatial dispersion [51] can be excluded as all calculations were carried out at normal incidence.

The regions with strong optical chirality form four main lobes originating from the sides of the antenna with alternating handedness of the chiral fields. At the front of the structure, four smaller regions with opposite handedness than the corresponding main lobes occur additionally. Due to the symmetry of the configuration, the integral over optical chirality in each slice normal to the propagation direction of the incident light vanishes.

Compared to the distribution of electric field enhancement (shown in Fig. 1(b)) the shapes of the respective fields are different. Hence, the formation and enhancement of chiral fields are no direct consequence of electric field enhancement alone. The chiral near-fields can also not be explained by just the scattered field of the antenna. Analysis of the fields of the fundamental mode of the antenna calculated by a FMM mode solver [52] without an external stimulus yields no optical chirality, as the respective electric and magnetic fields are orthogonal. For a proper explanation the incident field has to be taken into account. The generated optical chirality is a result of the interference between incident and scattered fields.

3. Dipole model for the generation of chiral fields

To demonstrate the underlying mechanism, we replace the nanoantenna with a point dipole. A Hertzian dipole directly supports the second prerequisite for chiral fields because the electric and magnetic fields feature a perfect phase difference of $\pi/2$ in the near-field. Nevertheless, the field lines are orthogonal at each point in space, leading to no optical chirality at all. In the presence of an external driving field, however, the lines can become distorted in a way such that optical chirality occurs.

We model the incident electromagnetic field as an arbitrary polarized plane wave propagating in z-direction:

$$\mathbf{E}_{\mathrm{in}} = E_0 \mathbf{J} e^{ikz}\,, \tag{3}$$

$$\mathbf{B}_{\mathrm{in}} = \frac{1}{c}\left(\mathbf{e}_z \times \mathbf{E}_{\mathrm{in}}\right). \tag{4}$$

Here, E_0 is the electric field amplitude, k the wave number, c the vacuum velocity of light, and $\mathbf{e}_z$ describes the unit vector in z-direction. The polarization state is determined by the Jones vector $\mathbf{J}$. The induced dipole fields close to the antenna can be approximately described by [53]

$$\mathbf{E}_{\mathrm{d}}(\mathbf{r}) = \frac{1}{4\pi\varepsilon_0}\frac{3\mathbf{n}(\mathbf{p}\cdot\mathbf{n})-\mathbf{p}}{r^3}\cdot\chi\,, \tag{5}$$

$$\mathbf{B}_{\mathrm{d}}(\mathbf{r}) = \frac{\mu_0}{4\pi} ik \frac{c}{r^2}\left(\mathbf{r}\times\mathbf{p}\right)\cdot\chi\,. \tag{6}$$

Here, ε_0 and μ_0 are the permittivity and permeability of vacuum, respectively. $\mathbf{n} = \mathbf{r}/r$ is the normal vector, $\mathbf{p}$ is the dipole vector that describes the orientation of the dipole in space.

#176581 - $15.00 USD Received 20 Sep 2012; revised 31 Oct 2012; accepted 1 Nov 2012; published 7 Nov 2012

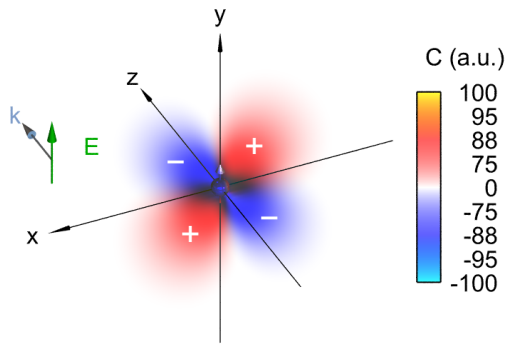

Fig. 2. Distribution of optical chirality near a dipole driven by an external field. A highly symmetric pattern is formed. The plot uses a nonlinear color scale to obtain better contrast.

The coupling term χ accounts for the fact that the dipole is driven by an external field:

$$\chi = \frac{\mathbf{E}_{\text{in}} \cdot \mathbf{p}}{|\mathbf{E}_{\text{in}}|} e^{i\frac{\pi}{2}} . \tag{7}$$

It accounts for two things: Firstly, only components of the electric field parallel to the dipole axis can excite the dipole. Secondly, a phase shift of $\pi/2$ between the incident electric field and the electric field of the dipole is introduced according to theoretical predictions for plasmonic antennas driven at resonance frequency [54, 55].

Using this model the optical chirality of a driven Hertzian dipole can be calculated as

$$C_{\text{d}} = -\frac{\varepsilon_0 \omega}{2} \text{Im}\left[(\mathbf{E}_{\text{in}} + \mathbf{E}_{\text{d}})^* \cdot (\mathbf{B}_{\text{in}} + \mathbf{B}_{\text{d}})\right] = C_{\text{in}} - \frac{\varepsilon_0 \omega}{2} \left[\text{Im}(\mathbf{E}_{\text{in}}^* \cdot \mathbf{B}_{\text{d}}) + \text{Im}(\mathbf{E}_{\text{d}}^* \cdot \mathbf{B}_{\text{in}})\right] . \tag{8}$$

Here, C_{in} is the optical chirality of the incident electromagnetic field. $\mathbf{E}_{\text{d}}^* \cdot \mathbf{B}_{\text{d}}$ vanishes as the electric and magnetic field lines of the undistorted dipole are orthogonal. Therefore, the electromagnetic near-field of the dipole alone is achiral at every point in space.

This simple model cannot be used for a quantitative analysis as important aspects such as dipole strength or absorption in the antenna are not taken into account. Nevertheless, it is useful to obtain more general insight into the principles behind generation and enhancement of fields with nonzero optical chirality.

3.1. Incident light with polarization parallel to the dipole axis

Figure 2 shows the calculated optical chirality for a dipole oriented in *y*-direction. The obtained values have been plotted in a logarithmic scale for better contrast. The incident light was also *y*-polarized. This corresponds to the situation in Fig. 1(a) where a linear antenna was driven by linearly polarized light. In both the simulation and the dipole model one recognizes the four main lobes with alternating sign of optical chirality (and thus alternating handedness of the chiral fields) around the scatterer. In this way, the simple Hertzian dipole is a good model for the plasmonic nanoantenna. Nevertheless, the additional distortions at the front of the structure are not accounted for in the model. Hence, they should be related to the finite dimensions of the plasmonic antenna.

To understand the fundamental behavior behind the generation of chiral fields by a linear antenna, we evaluate Eq. (8) using the Jones vector of linearly polarized light. $\text{Im}(\mathbf{E}_{\text{in}}^* \cdot \mathbf{B}_{\text{d}})$ vanishes as the magnetic field component parallel to the dipole axis is zero. As linearly polarized

#176581 - $15.00 USD Received 20 Sep 2012; revised 31 Oct 2012; accepted 1 Nov 2012; published 7 Nov 2012

light features no optical chirality, one obtains

$$C_{\mathrm{d}}^{\mathrm{lin}} = -\frac{\varepsilon_0 \omega}{2} \mathrm{Im}(E_{\mathrm{d,x}}^* \cdot B_{\mathrm{in,x}}) \,. \tag{9}$$

This equation shows that the induced optical chirality is due to an interaction of the magnetic field of the incident light, which is only present in x-direction, with the scattered electric field of the dipole. As the incident magnetic field of the incoming plane wave is uniform, the four lobes and their alternating signs are a result of the distribution of the x-component of the dipole field. It changes indeed sign at each quadrant of the x,y-plane. For each point on that plane the sign is independent of z. Also, strongest values of E_{x} occur at lines with an angle of 45° with respect to the coordinate axis while this component vanishes at the x- and y-axis. Therefore, the shape of the chiral fields can be explained just by geometric considerations.

Note that one quantity determining the values of optical chirality is the field enhancement due to the dependence of $C_{\mathrm{d}}^{\mathrm{lin}}$ on the scattered electric field. Hence, one way to increase the optical chirality would be to alter the design in a way that the field enhancement is increased. Nevertheless, the dipolar character of the scattered fields must be maintained to keep our simple model applicable.

3.2. Incident light with circular polarization

For incident circularly polarized light, which already exhibits nonvanishing optical chirality itself, we have

$$\mathbf{E}_{\mathrm{in}} \propto \frac{1}{\sqrt{2}} \begin{pmatrix} 1 \\ \pm i \\ 0 \end{pmatrix} \quad \text{and} \quad \mathbf{B}_{\mathrm{in}} \propto \frac{1}{\sqrt{2}} \frac{1}{c} \begin{pmatrix} \mp i \\ 1 \\ 0 \end{pmatrix} . \tag{10}$$

We start the evaluation of Eq. (8) with a discussion of $\mathrm{Im}(\mathbf{E}_{\mathrm{d}}^* \cdot \mathbf{B}_{\mathrm{in}})$. As the x- and y-component of the incident magnetic field are $\pi/2$ out of phase while all components of the electric field of the dipole are in phase, only one of the two terms obtained in the scalar product can contribute to optical chirality. Careful examination yields that this is indeed the x-component as in the case of linearly polarized incident light.

We get an additional contribution from $\mathrm{Im}(\mathbf{E}_{\mathrm{in}}^* \cdot \mathbf{B}_{\mathrm{d}})$ due to the nonvanishing x-component of the incident electric field. As $B_{\mathrm{d,y}}$ is still zero the optical chirality of the Hertzian dipole driven by circularly polarized light can be written as

$$C_{\mathrm{d}}^{\mathrm{CPL}} = C_{\mathrm{d}}^{\mathrm{lin}} + C_{\mathrm{in}}^{\mathrm{CPL}} - \frac{\varepsilon_0 \omega}{2} \mathrm{Im}(E_{\mathrm{in,x}}^* \cdot B_{\mathrm{d,x}}) \,. \tag{11}$$

$C_{\mathrm{in}}^{\mathrm{CPL}}$ denotes the intrinsic optical chirality of circularly polarized light while $C_{\mathrm{d}}^{\mathrm{lin}}$ is the distribution of optical chirality obtained for linearly polarized incident light (cf. Eq. (12)). Hence, switching from linearly to circularly polarized light only adds additional terms to the response for linearly polarized light.

The three terms behave differently when the handedness of the incident circular polarization is changed. Firstly, $C_{\mathrm{d}}^{\mathrm{lin}}$ does not depend on the handedness of the incident field as it occurs already for linear polarization. The sign of $C_{\mathrm{in}}^{\mathrm{CPL}}$, which originates from the incident field alone, differs for the two different polarizations. The third term requires more detailed analysis: In our description, the scattered fields of the dipole exhibit a sign flip when the handedness of the incident polarization is switched while the incident polarization does not (cf. Eq. (10). Therefore, the third term also flips its sign when the incident polarization changes. One can deduce from the symmetry of the x-component of the induced magnetic field that the third term additionally changes its sign between the two half spaces defined by the x,y-plane.

#176581 - $15.00 USD Received 20 Sep 2012; revised 31 Oct 2012; accepted 1 Nov 2012; published 7 Nov 2012

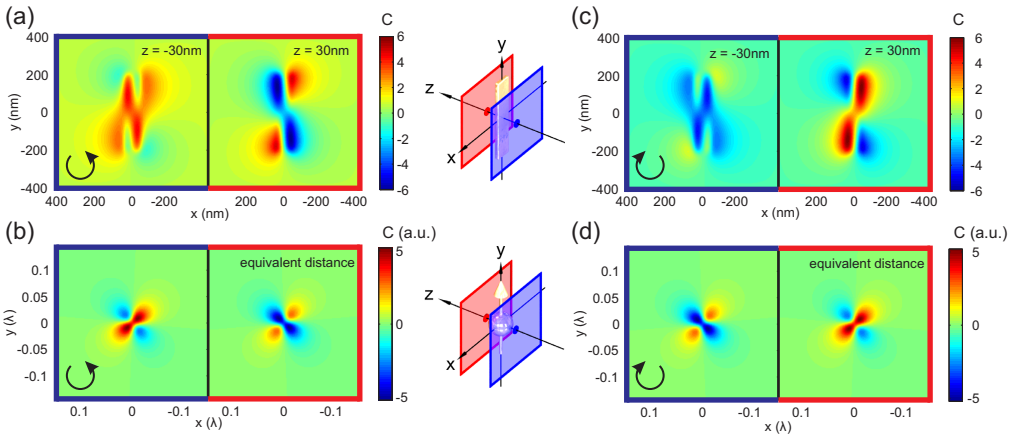

Fig. 3. Optical chirality induced by circularly polarized light near a linear plasmonic nanoantenna (a, c) compared to the dipole model (b, d). Slices were taken 30 nm before (blue border) and after (red border) the structure. The distribution of optical chirality is similar to the case of incident linearly polarized light (cf. Figs. 1(a) and 2) with some of the lobes being stronger for circularly polarized light. One can find a nice symmetry between incident left-handed (a, b) and right-handed (c, d) circularly polarized light as well as between the slices in front and behind the structure. The dipole model resembles the qualitative distribution of optical chirality very well. Nevertheless, some additional distortions occur at the front of the structure (also occuring in the plot in Fig. 1(a)) that cannot be explained by this simple model.

Due to this sign flip, the volume integral over the third term in Eq. (11) vanishes. Thus, the volume integral of the optical chirality in this configuration is determined by the optical chirality of the incident light. This finding is consistent with the intuitive imagination that the presence of an achiral structure should only induce local changes that vanish when integrated over all space.

Figure 3 shows the behavior of a linear plasmonic nanoantenna at its fundamental plasmon resonance for circularly polarized incident light in both simulation as well as the dipole model. Slices normal to the propagation direction 30 nm in front and behind the structure are shown to obtain a better comparison of the different scenarios. The equivalent distance in wavelength units has been used for the z-distance in the dipole model. Note that the x- and y-axis do not correspond to the scales used to plot the simulations. This can be related to the finite dimensions of the plasmonic antenna, which cannot be taken into account using our model.

One can clearly identify the four main lobes that already occured for linearly polarized incident light. As discussed, these lobes experience no sign flip when the handedness of the incident polarization is switched. Due to the circularly polarized incident light, two opposing lobes are slightly connected. The pair of lobes forming this connection changes depending on the handedness of the incident light as well as the z-position. The changing response in the slices in front and behind the structure is a clear indication that the third term in Eq. (11) dominates over the optical chirality of the circularly polarized incident light that only adds a constant value independent of the spatial position.

Figure 3 also demonstrates that the influence of $C_{\mathrm{d}}^{\mathrm{lin}}$ is indeed strong as it determines the general shape of the chiral near-fields. Next to the structure, where optical chirality is strongest, the second and third term in Eq. (11) induce only minor changes to the chiral field distributions. For larger distances, however, the difference for the two excitations becomes more pronounced.

#176581 - $15.00 USD Received 20 Sep 2012; revised 31 Oct 2012; accepted 1 Nov 2012; published 7 Nov 2012

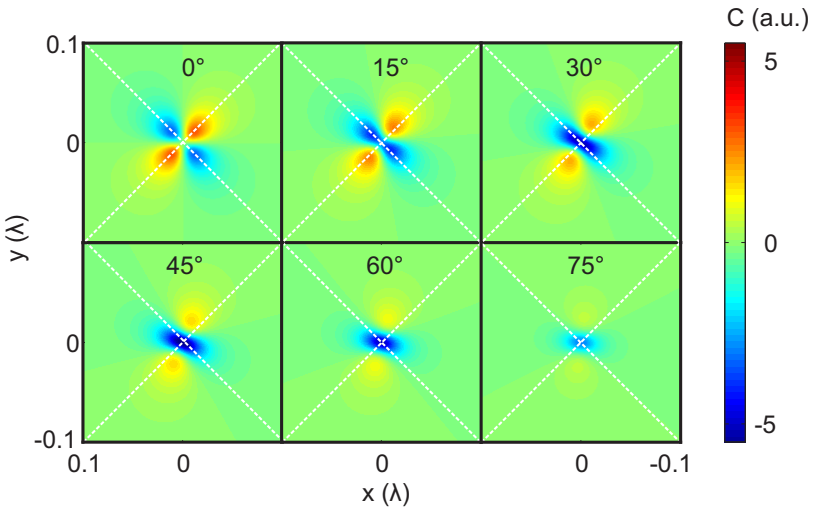

Fig. 4. Optical chirality of a Hertzian dipole illuminated with linearly polarized light at a distance of $z = 0.02\,\lambda$ behind the dipole. The distribution changes with increasing polarization angle. The white dashed lines are guides to the eye to see the rotation of the initial lobes of optical chirality.

Nevertheless, the absolute values of optical chirality decreases with increasing distance.

This behavior can also be understood through our dipole model as $C_\mathrm{d}^\mathrm{lin}$ is determined by the electric field of the dipole while the magnetic field enters the third term of Eq. (11). The electric near-field is stronger but decays faster than the magnetic field of the Hertzian dipole as can be seen from Eqs. (5) and (6).

This distance-dependent difference of the single contributions to optical chirality leads to the interesting effect that three-dimensional maps of optical chirality for circularly polarized incident light look similar as the one shown in Fig. 1(a) for linearly polarized light. Close to the structure, the contribution of $C_\mathrm{d}^\mathrm{lin}$ dominates while for larger distances optical chirality becomes too small to be visible in the map.

The field plots generated by the dipole model (cf. Fig. 3) resemble the simulated results with good agreement. The general behavior of the plasmonic antenna illuminated with circularly polarized light can be explained qualitatively: only the distortions at the front cannot be found in the model, which was also the case for linearly polarized incident light.

3.3. Linearly polarized incident light with arbitrary polarization angle

A third configuration, which is different from both illumination schemes discussed thus far, is linearly polarized light with a nonzero angle φ between the electric field and the dipole axis. As in the case of circularly polarized light both the *x*- and *y*-component of the incident fields are present. The difference is the absence of the $\pi/2$ phaseshift for the single components of each field. Therefore, $\mathbf{E}_\mathrm{in}$ and $\mathbf{B}_\mathrm{d}$ are in phase and the corresponding term in Eq. (8) vanishes. In exchange, the *y*-component of the incident magnetic field and the electric field of the dipole are out of phase and therefore contribute to optical chirality.

As a result, we obtain

$$C_\mathrm{d}^\varphi = C_\mathrm{d}^\mathrm{lin} - \frac{\varepsilon_0 \omega}{2} \mathrm{Im}(E_\mathrm{d,y}^* \cdot B_\mathrm{in,y})\,. \tag{12}$$

This equation might look similar to the results we analyzed before. Nevertheless, there is a crucial difference: for the first time also the *y*-component of the fields, which is the component

#176581 - $15.00 USD Received 20 Sep 2012; revised 31 Oct 2012; accepted 1 Nov 2012; published 7 Nov 2012

parallel to the dipole axis, contributes to optical chirality. Also, both contributing terms are of the same magnitude at each distance. For the case of circularly polarized light, one could still interpret the plots as a superposition of $C_{\mathrm{d}}^{\mathrm{lin}}$ and some additional components. This picture becomes more complicated for linearly polarized light with arbitrary polarization angles (cf. Fig. 4): We do still find connected lobes as in the case of circularly polarized incident light. But now in addition the whole configuration is rotated. The absolute values of optical chirality increase with increasing polarization angle (up to a maximum at $\varphi = 45^\circ$). The values decrease for larger angles as the excitation of the dipole decreases as well with vanishing optical chirality at $\varphi = 90^\circ$. Note that the angle with maximum optical chirality depends strongly on the excitation efficiency of the dipole which is not explicitly taken into account in our simple model.

As a result we find that circularly polarized incident light leads to quite similar distributions of optical chirality as light polarized parallel to the dipole axis. However, the picture becomes more complicated as soon as the polarization direction is rotated.

4. Novel scheme for chiroptical spectroscopy

Based on our theoretical findings, we propose the following measurement scheme: We consider a gold square instead of the linear antenna previously analyzed. For incident light with linear polarization in *y*-direction, essentially the same distribution of optical chirality as for the linear antenna shown in Fig. 1(a) occurs with only minor differences due to the different dimensions (cf. Fig. 5(a)). In contrast to the case of the antenna, the incident light here is also in resonance with the structure for the orthogonal polarization. In this case, the pattern of optical chirality is just twisted by 90° as shown in Fig. 5(b). At each position in space the sign of optical chirality changes for the two different linear polarizations.

The excitation of chiral molecules depends on the value of optical chirality [36]. Thus, we expect a difference in absorption for the two linear polarizations when placing a molecule in one of the four main lobes. This will not occur without the nanosquare as the absorption of linearly polarized light by an isotropic distribution of chiral molecules is independent of the polarization angle.

Nevertheless, it is important to deposit molecules only onto regions with the same sign of optical chirality. If the complete square were covered homogeneously with molecules, the difference in absortion would be expected to vanish when averaged over a large area. To obtain this, we suggest a design as shown in Fig. 5(c): Starting from an array of gold nanosquares, an additional layer is added. In this layer, diagonal stripes block the access to two opposite corners of the square. Thus, only one handedness of the generated chiral near-field is accessible for molecules. One can get rid of the distortions at the front of the structure by illuminating the sample from the bottom. Then the substrate prevents accessing these areas.

This geometry should in principle allow circular dichroism type measurements with linearly polarized light. Conventional circular dichroism spectroscopy measures the difference in absorption of left- and right-handed circularly polarized light. In our geometry, chiral fields of opposite handedness are instead generated by linearly polarized incident light impinging on the nanosquares. Chiral molecules placed in a groove interact with only one polarity of the resulting difference in optical chirality as depicted in the close-up in Fig. 5(c).

Spectroscopic measurements employing linearly polarized light are simpler than those using circularly polarized light as no broadband circular polarizer is needed. We suggest to match the refractive index of the chiral medium to that of the the top layer to suppress contributions from a refractive index grating. Nevertheless, additional investigations to estimate the sensitivity of our proposed device compared to common circular dichroism measurement schemes are necessary. The higher optical chirality relative to a circularly polarized plane wave (cf. Fig. 5 that shows

#176581 - $15.00 USD Received 20 Sep 2012; revised 31 Oct 2012; accepted 1 Nov 2012; published 7 Nov 2012

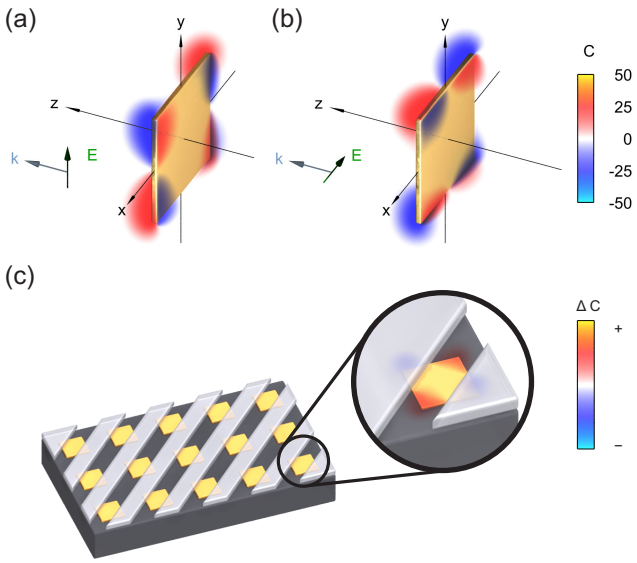

Fig. 5. (a) Using a square instead of the linear antenna yields similar results for incident light polarized in *y*-direction at a frequency of 268 THz. (b) When the orthogonal polarization is used, the incident light is still in resonance with the square which leads to the same pattern of optical chirality but rotatet by 90°. Note that the scale of the color bar is only half as big as for the linear antenna shown in Fig. 1(a). (c) When only two opposite corners are accessible by chiral molecules this geometry could be used for circular dichroism type measurements but with incident linearly polarized light to experimentally verify our theoretical findings. The close-up shows the calculated difference in optical chirality for the two different incident polarizations. Only one handedness of the chiral fields can be accessed.

this increase due to the normalization discussed in Section 2) already indicates an enhancement of the sensitivity.

5. Conclusion

In conclusion, we have shown that a geometrically achiral configuration, namely the illumination of a linear plasmonic nanoantenna with linearly polarized light at normal incidence, will generate chiral near-fields. We have demonstrated that it is sufficient to analyze a driven Hertzian dipole to explain the resulting field distributions. Using this simple model, the general chiroptical near-field response of the linear antenna for different incident polarization states can be understood qualitatively. Additionally, we have proposed an experimental setup to verify our findings, which leads to a novel scheme for chiroptical spectroscopy using linearly instead of circularly polarized light. Future research will analyze the quantitative capabilities of such sensing devices. Additionally, our dipole model will be extended to analyze structures with more complex geometries in the future.

Acknowledgment

The authors thank Jens Dorfmüller and Thomas Weiss for helpful discussions and Sven Hein for help with the visualization. This work was financially supported by BMBF (13N9048 and 13N10146), DFG (SPP1391 and GI 269/11-1), BW Stiftung (Spitzenforschung II), and MWK BW (Az: 7533-7-11.6-8). This work was supported by the German Research Foundation (DFG) within the funding program Open Access Publishing.

#176581 - $15.00 USD Received 20 Sep 2012; revised 31 Oct 2012; accepted 1 Nov 2012; published 7 Nov 2012